Support Structure Constrained Topology Optimization for Additive Manufacturing

Amir M. Mirzendehdel, Krishnan Suresh

Department of Mechanical Engineering, University of Wisconsin, Madison, WI 53706, USA

HIGHLIGHTS

- Addresses additive manufacturing support structure constraint in topology optimization
- Introduces topological sensitivity for support structures
- Combines support structure sensitivity with performance sensitivity
- Proposes a robust and efficient algorithm for support structure constrained topology optimization

ABSTRACT

There is significant interest today in integrating additive manufacturing (AM) and topology optimization (TO). However, TO often leads to designs that are not AM friendly. For example, topologically optimized designs may require significant amount of support structures before they can be additively manufactured, resulting in increased fabrication and clean-up costs.

In this paper, we propose a TO methodology that will lead to designs requiring significantly reduced support structures. Towards this end, the concept of 'support structure topological sensitivity' is introduced. This is combined with performance sensitivity to result in a TO framework that maximizes performance, subject to support structure constraints. The robustness and efficiency of the proposed method is demonstrated through numerical experiments, and validated through fused deposition modeling, a popular AM process.

Keywords:
Topology optimization
Additive manufacturing
3D printing
Support structure
Topological sensitivity
Level-set

1. Introduction

Topology optimization (TO) represents a class of *computational methods* for designing light-weight, high-performance structures [1], [2], [3]. After several years of intensive research, it has emerged as a powerful design tool, and is deployed in optimization of aircraft components [4], [5], spacecraft modules [6], automobiles components [7], cast components [8], compliant mechanisms [9], etc.

Additive manufacturing (AM), on the other hand, represents a class of *manufacturing processes* for fabricating parts through material addition [10], [11]. The growing interest in AM stems from its ability to fabricate highly complex parts with relative ease.

Although TO and AM have flourished independent of each other, there is significant interest today in integrating the two for several reasons [12]–[16]:

1. Designs stemming from TO are geometrically complex, and therefore hard to manufacture using traditional processes. However, these designs can often be additively manufactured; Figure 1a, for example, illustrates a structural design problem that is optimized through TO (Figure 1b), and then fabricated using AM (Figure 1c), with minimal human interference.
2. Since fabrication cost in AM is proportional to the material used, light-weight topology optimized designs are particularly relevant in AM.

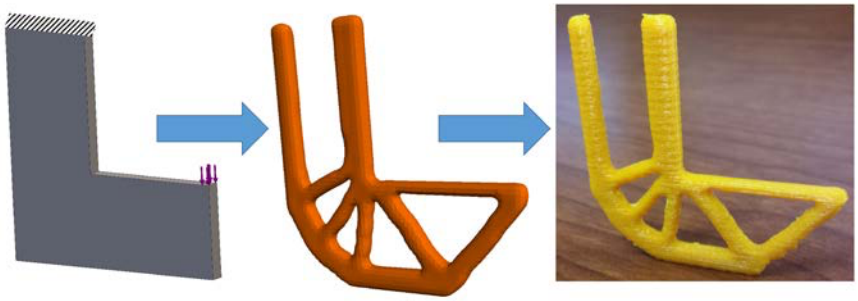


Figure 1: (a) A structural problem. (b) Topology optimized design. (c) AM fabricated part.

In theory, these and other characteristics make TO and AM well suited for each other. However, in practice, topologically optimized designs are often not AM friendly [16], [12]. For example, consider the structural problem posed in Figure 2a. A topologically optimized design is illustrated in Figure 2b; observe the four 'props' that improve the structural rigidity but are overhanging (see Section 3.1 for a formal definition of overhanging). These props will require additional support structures to prevent drooping' (in AM polymer processes) and 'burning' (in metal AM processes). Figure 2c illustrates an AM built part with these additional support structures.



Figure 2: (a) Structural problem. (b) Optimized topology. (c) Fabricated part with support structures.

Support structures directly add to the build-time and material cost. Material costs can be substantial in AM; for example, the largest percentage cost for metal AM, besides the machine cost that is amortized, is material cost (18%) [17]. Further, support structures can be hard to remove (and sometimes even inaccessible), leading to the *post-fabrication (clean-up) cost*. Post-fabrication costs make-up for about 8% of AM product cost [17].

The objective of this paper is to develop a TO methodology for limiting the support structure volume, thereby leading to designs that are AM friendly. In Section 2, prior research on support structure minimization is reviewed, followed by a review on recent TO advances. In Section 3, the concept of "topological sensitivity for support structures" is introduced, and a methodology to impose support structure constraint during TO is proposed. In Section 4, the efficacy of the proposed methodology is demonstrated through benchmark studies. Section 5 summarizes the contributions of this paper, and discusses future work.

2. Literature Review

For reasons stated earlier, support structure minimization is of significant interest within the AM community, and several methods have been proposed. These are classified into the following categories.

Strategy 1: Finding an optimal build direction

AM build-direction can have a significant impact on support structures. Therefore, a popular strategy is to find a build-direction that minimizes support structure volume (and optionally optimizes other AM metrics). For instance, Jibin [18] developed a multi-objective function to find an optimal build direction to minimize volumetric error, support structure, and build time. Along similar lines, Pandey et al. [19] proposed a multi-criteria genetic algorithm to minimize support structure and build time, while improving surface quality. In both instances, weighted averaging was used to solve multi-objective problems. Nezhad et al. [20] proposed tracing the Pareto front to find the optimal part orientation; the Pareto front involved two objective functions, namely support structure and build time. Paul and Anand [21] used a voxel representation (rather than the STL representation) to minimize support structure while satisfying constraints on cylindricity and flatness errors. More recently, Das et al. [22] identified optimal build orientation with respect to tolerance errors and support structure volume by extracting product manufacturing information. Alternate approaches for selecting build-direction include optimizing post-build quality and perception [23], and increased (cross-sectional) mechanical strength [24].

Strategy 2: Generating efficient support structures

While the above methods assume vertical support columns, more efficient support structures have been proposed for a given build-direction. For example, the commercial software Meshmixer™ generates tree-like support structures. While this potentially reduces the support volume, manual

modifications are required to ensure printability. Vanek et al. [25] overcame this deficiency by presenting an efficient method for automatically creating tree-like support structures that are printable. Specialized methods have also been proposed for specific AM processes. For instance, Barnett and Gosselin [26] developed shell and film techniques to create support structures for processes with weak support materials, such as three dimensional foam printers. Dumas et al. [27] exploited scaffolding structures to generate efficient supports for Fused Deposition Modeling (FDM). Considering the stability of the object throughout the build process, the method first identifies support points and then creates horizontal bars between vertical pillars to reduce the support volume. A contour-based support generation scheme was proposed in [28] based on layer-wise analysis. The method first analyzes all of the layers and then generates support anchors using offset and Boolean operations to ensure printability of the part.

Strategy 3: Following design rules for AM

A third strategy is to include support volume constraints during the *manual* design process [29]–[33]. This is often based on design rules such as [30]: (1) avoid surfaces with large overhang angle, (2) avoid large-size holes (say, larger than 5 mm) [22] perpendicular to the build-direction, (3) avoid trapped surfaces where support structures are hard to remove, and (4) use explicit fillets and chamfers to avoid support structures. Since these rules are feature-based, they are hard to include during TO.

Strategy 4: Optimizing the topology for AM

The final strategy is to include AM constraints within TO. As stated earlier, the advantage of this strategy lies in the (potential) integration of these two technologies.

Imposing manufacturing constraints in TO has been addressed before; a particularly relevant constraint is that of 'draw-direction constraint' for casting [34], [35], where the TO algorithm was

modified so as to avoid ‘inserts’. While this is analogous to the support structure constraint, there are two fundamental differences: (1) support structures are governed by a threshold angle (see Section 3.1) while the threshold angle for draw-direction is essentially zero, and (2) the draw-direction constraint is bidirectional, while the build-direction in AM is unidirectional. Thus, the draw-direction methodology does not apply to AM; novel methods are needed.

Bracket et. al. [12] made several recommendations on integrating TO and AM,. For example, to minimize support structures, they suggested a penalization scheme on overhanging surfaces, and an edge analysis was carried out on a benchmark 2D example. The overhang constraint was suggested but not demonstrated.

Wang et. al. [36], proposed a novel strategy to reduce the material cost by first extracting the frame structure of the design. The frame is in fact the solution of a multi-objective optimization problem that minimizes the number of struts while considering stability and printability.

Leary [14] introduced the idea of self-supporting designs, where the TO optimized design was altered to include features similar to support structures. In other words, support structures were introduced as design features *a posteriori*. Since this is carried out after TO, the structural load path is altered, and may violate stress and other performance constraints.

Based on the suggestions proposed by Bracket [12], Gaynor and Guest [16], employed a smooth Heaviside approximation to penalize overhanging surfaces within a SIMP based TO. They demonstrated that, for 2D compliance minimization, this scheme changes the topology to be AM friendly. Specifically, they demonstrated that it is possible to eliminate support structures by suitably changing the TO process. The results are encouraging, but they noted convergence issues when the overhanging penalization was imposed. Recently, Hu et. al [37] proposed a shape optimization technique to alter the model to a more self-supported one. To this end, once a

volumetric tetrahedral mesh is generated, the overhang tetrahedra are mapped onto the Gauss sphere and minimally rotated to a self-supported state; the method was also proven to be effective in finding optimal build direction.

3. Proposed method

While we are witnessing significant research activities in TO and AM, a robust framework for integrating the two is lacking. The focus of this paper is to address one aspect of integrating TO and AM, specifically, minimizing support structures.

Consider a typical compliance minimization problems of the form:

$$\begin{aligned} &\underset{\Omega \subset \Omega_0}{Minimize}\, J \\ &|\Omega| \leq V_f |\Omega_0| \\ &\mathbf{Kd} = \mathbf{f} \end{aligned} \tag{1}$$

In Equation (1), $J = \mathbf{f}^T \mathbf{d}$ is the compliance that must be minimized, $|\Omega_0|$ is the initial design volume, Ω is the topology to be computed, and V_f is the desired volume fraction; $\mathbf{K}$ is the stiffness matrix, f is the external force vector, and d is the displacement vector.

3.1 The PareTO level-set method

There are several TO methods employed today to solve such TO problems; these include Solid Isotropic Material with Penalization (SIMP) [38]–[41], level-set [42], [42]–[44] and evolutionary [45] methods. Among these, we propose to use the level-set based *Pareto Topology Optimization* (PareTO) method [46]–[48] for the following reasons: (1) in level-set methods, the boundary is well-defined at all times, making it easier to impose support structure constraints, and (2) PareTO relies on the *topological sensitivity* concept (described in section 3.4) that applies to various

performance criteria and constraints, and can be generalized to handle support sensitivity, as discussed in the remainder of the paper.

An important feature of the PareTO method is that it generates Pareto-optimal topologies for various volume fractions. To illustrate, consider the three-hole bracket of Figure 3, where the two left side holes are fixed and the right hand side hole is subject to a downward unit load. The underlying material is assumed to be isotropic ABS plastic with Young's modulus of $E = 2\text{GPa}$ and Poisson ratio of $\nu = 0.39$.

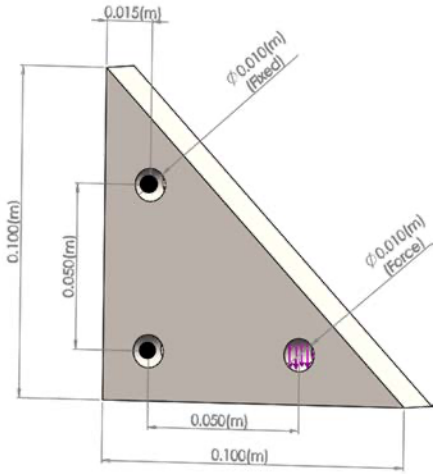


Figure 3: Three-hole bracket.

Figure 4 illustrates the progression of the optimization process in PareTO up to a volume fraction of 0.5. Observe that optimization begins with a volume fraction of 1.0, and generates multiple topologies that lie on the Pareto curve (Pareto tracing). This will play an important role in the proposed method for constraining the support structure volume. Further, we do not rely on a velocity field concept to move the boundary; instead, we use fixed-point iteration, proposed by [49], to converge to Pareto-optimal designs; the implementation is described in [46]–[48].

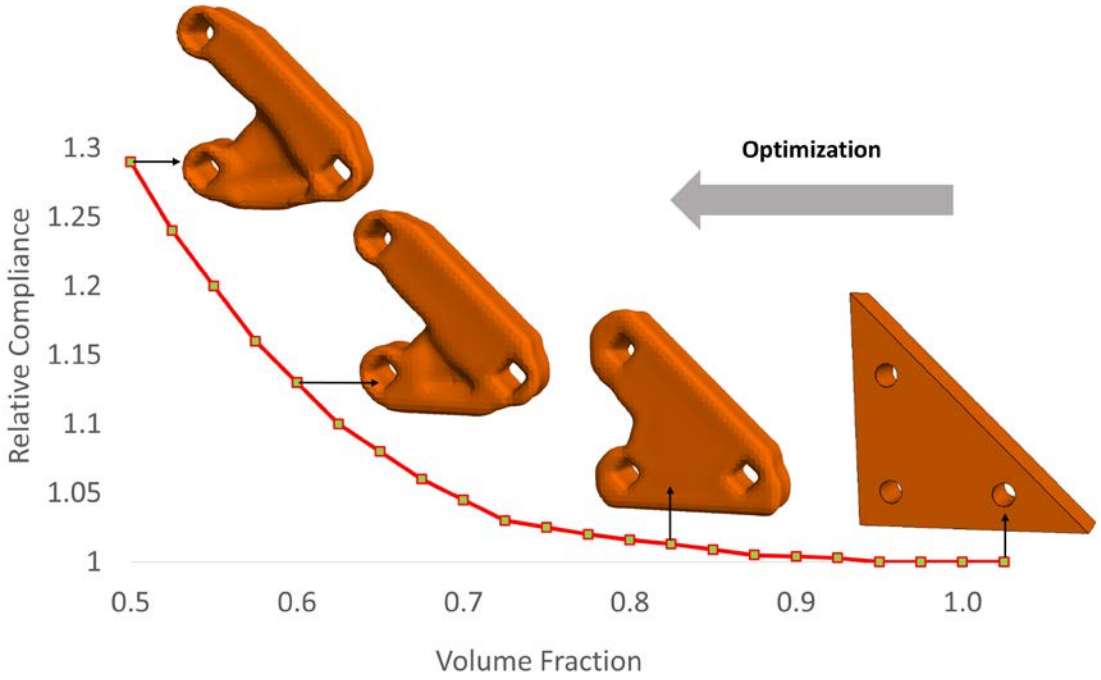


Figure 4: Pareto curve for three-hole bracket optimization.

3.2 Limitations of the Overhang Constraint

Before we discuss how support structure constraints can be imposed, we will briefly review how support structures are algorithmically generated. This will provide key insights into developing appropriate constraints.

Support structure generation in AM is based on the overhang concept which states that *if the angle between the boundary normal and the build direction exceeds a certain threshold, then support structures are needed at that point* [12]. For instance, for the design and the build-direction illustrated in Figure 5a, the subtended angle α is illustrated in Figure 5b. Given a threshold $\hat{\alpha}$ (typically around 135^0), boundary points with $\alpha > \hat{\alpha}$ are considered overhanging, and require support, as illustrated in Figure 5c; For simplicity, vertical support structures are assumed in this paper; support structures may terminate at the platform or at any opposing non-overhanging point. The union of all such support structures results in a support volume as illustrated in Figure 5d. The fill-ratio, i.e., material density, of support structures is typically less than that of the primary design.

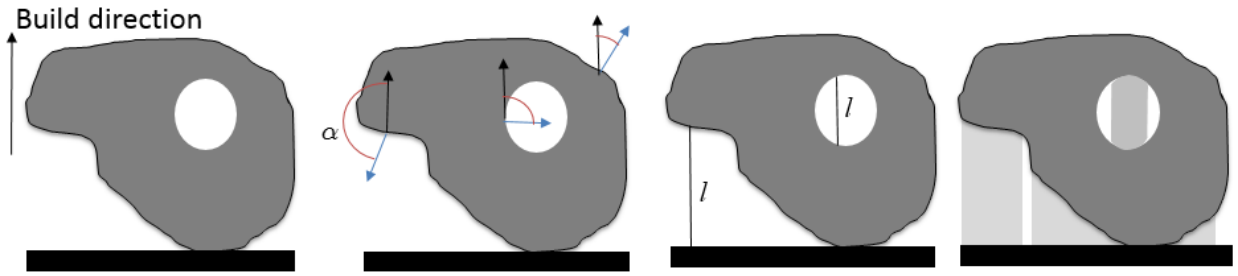


Figure 5: (a) Build-direction. (b) Subtended angle. (c) Support length. (d) Support volume.

The above definition is exploited both by designers and software algorithms to create suitable support structures; for example, see [25]. Further, the definition suggests that if one could *eliminate all overhanging surfaces*, then support structures can also be eliminated. But, this is not an effective optimization strategy for the following reasons:

1. *Eliminating all overhanging surfaces may not be possible.* Researchers [16] have demonstrated that one can eliminate overhang surfaces in certain 2D problems. However this is unlikely to be successful in general, especially in 3D (as the numerical examples in Section 4 demonstrate). As was also suggested in [6], *"... there will probably be instances where it is not necessary for all support structure to be eliminated and so the user should be able to have some control over the strength of the penalty function."*.
2. *The overhang constraint does not penalize support volume.* Two overhanging surfaces with equal subtended angle will be penalized equally, although the support volume associated with one may be much larger than the other. To avoid such contradictions, a direct *constraint on the support volume* is desirable.
3. *Penalizing just the overhanging surfaces is insufficient.* Support volume may be enclosed between an overhanging surface and an opposing surface, as illustrated in Figure 6. To reduce support volume, both surfaces must be penalized, for example, by moving them closer to each other as illustrated. By penalizing the overhanging surface, only half the problem is addressed.

These limitations suggest that we must seek an alternate, and fundamentally different method to impose constraints on support structures during TO.

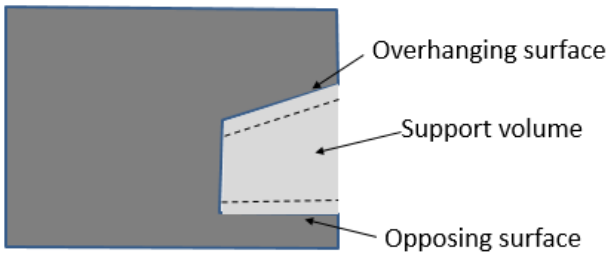


Figure 6: Moving either the overhanging or its 'opposing' surface changes the support volume.

We propose here a formulation that relies on (1) *dynamically estimating* the support volume as the topology evolves, and (2) imposing *constraints on the support volume through topological sensitivity methods*.

Consider the first step of dynamically estimating the support volume. In this paper, we assume that support structures are vertical. Therefore, the support volume is simply the integral of the support length over the boundary, multiplied by a suitable fill-ratio, (see Figure 5d), i.e.

$$S = \gamma \int_{\alpha \geq \hat{\alpha}} l_p \, d\Gamma \tag{2}$$

S : Support structure volume
α : Subtended angle
l_p : Length of support structure at boundary point p
γ : Fill ratio (relative material density) of support structures

In Equation (2), the exact value of the fill ratio γ is not critical; it can be assumed to be 0.5, without a loss in generality.

Further, for short overhangs, it is well known that support structures are not needed. For example, for FDM, the allowable overhang [12] can be approximated via:

$$h(mm) = \begin{cases} 5 + 40(1 - \alpha \,/\, \pi); & 3\pi/4 < \alpha \le \pi \\ \infty & 0 \le \alpha \le 3\pi/4 \end{cases} \tag{3}$$

Thus, at any point on the boundary, if the subtended angle is α, support structures are not needed if the overhang distance is less than h given by Equation (3). In the implementation, we search for self-supporting boundary within a distance given by Equation (3); see Figure 7.

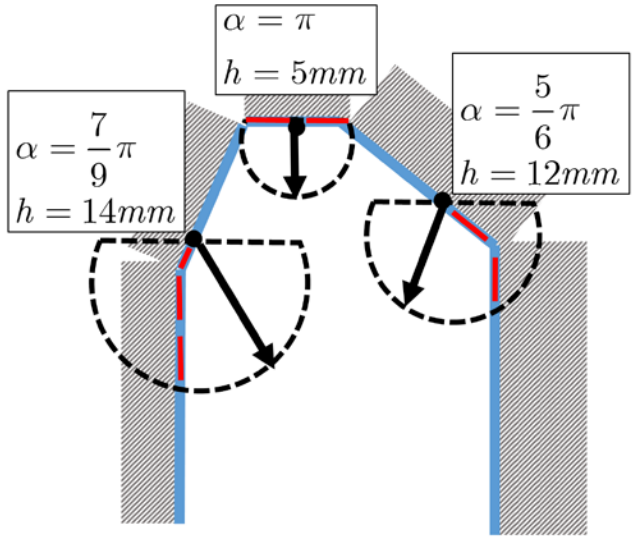


Figure 7: Searching for self-supporting boundary.

3.3 Options for Imposing Support Constraint

Next consider the challenge of imposing support volume constraint. Perhaps the simplest strategy is to impose an absolute constraint as in:

$$S \le S_{\max} \tag{4}$$

However, this places an unreasonable burden on the designer to arrive at an absolute value for the upper limit a priori. Instead, we consider relative upper bound constraints. Specifically, recall that in the PareTO method, one generates multiple topologies for various volume fractions, i.e., one can solve the unconstrained problem, and store reference support volumes $S_{unc.}(v)$ at intermediate volume fractions v. For example, Figure 8 illustrates the support volume $S_{unc.}(v)$ for the

unconstrained problem. The support volume curve is, in general, non-smooth, unlike the compliance curve in Figure 4.

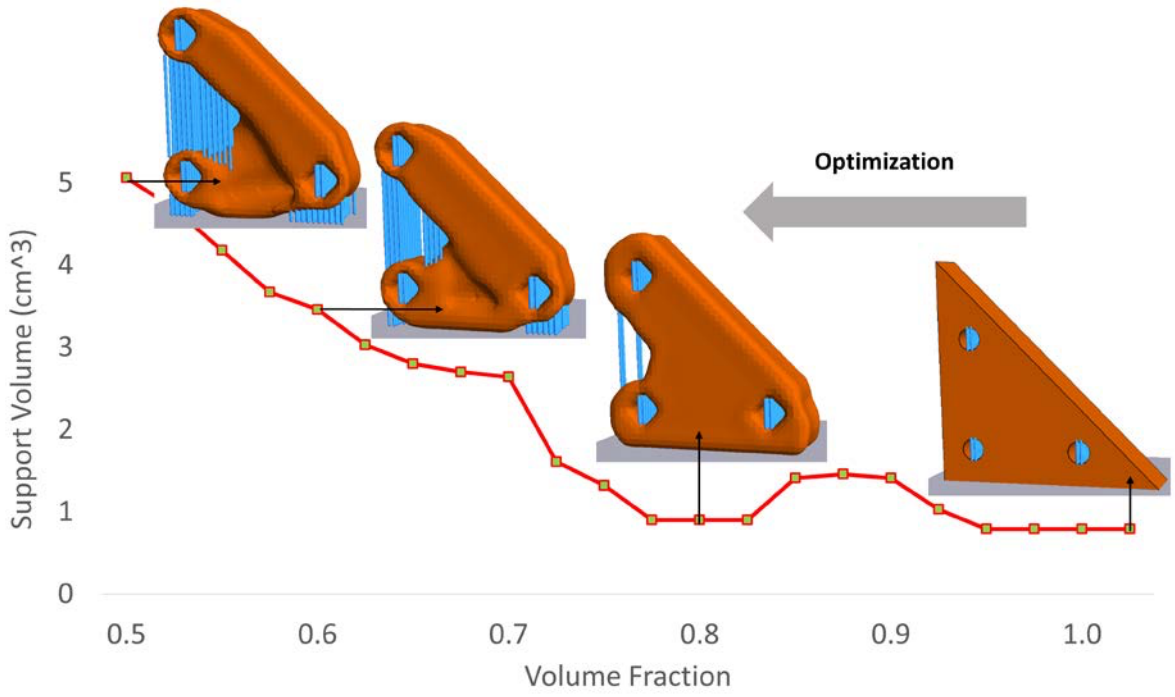


Figure 8: Relative support structure volume at different volume fractions for unconstrained problem.

Next we impose a relative constraint with respect to $S_{unc.}(v)$, via a user-defined parameter η ($0 < \eta \leq 1$)

$$S(v) \leq \eta S_{unc.}(v) \tag{5}$$

In other words, Equation (5) states that the desired support volume should be less than the unconstrained support volume by a factor of η , at each volume fraction (through interpolation, if necessary). Alternately, one can impose a constraint at the final volume fraction, but imposing a constraint at each volume fraction leads to a smoother optimization process. Further, in this paper, we treat Eq. (5) as a 'soft' constraint, i.e., the constraint is used to prioritize the solutions within the feasible space (see Section 3.6), rather than limiting this space [50].

In summary, we propose the following support-structure constrained TO problem, where the parameter η ($0 < \eta \leq 1$) is used to strike a balance between performance and AM costs (see numerical experiments in section 3.8):

$$\begin{aligned} &\underset{\Omega \subset \Omega_0}{Minimize}\, J \\ &\left|\Omega\right| \leq V_f \left|\Omega_0\right| \\ &S(v) \leq \eta S_{unc}(v)\ (soft) \\ &\mathbf{Kd} = \mathbf{f} \end{aligned} \tag{6}$$

In section 3.4, we consider a gradient based TO framework for solving the above problem. The framework will rely on topological sensitivity for performance [51]–[54], and the proposed topological sensitivity for support structure volume.

3.4 Topological Sensitivity of Performance

The PareTO method relies on the concept of topological sensitivity for driving the optimization process. To illustrate, consider the structural problem in Figure 9a that represents the design space Ω_0 . Consider now inserting a small *hypothetical* hole that modifies the topology (Figure 9b). Topological sensitivity is the rate of performance change of any quantity of interest φ with respect to the volumetric measure of the hole, i.e., in 2D,

$$\mathcal{T}_{\varphi}(p) \equiv \lim_{\varepsilon \to 0} \frac{\varphi(p;\varepsilon) - \varphi}{\pi \varepsilon^2} \tag{7}$$

If the performance metric is compliance, the field in 2-D is given by the closed-form expression [55]:

$$\mathcal{T}_{J}(p) = \frac{4}{1+\nu}\sigma : \varepsilon - \frac{1-3\nu}{1-\nu^2} tr(\sigma) tr(\varepsilon) \tag{8}$$

Thus the topological sensitivity can be computed as follows: (1) FEA is carried over the domain, (2) stresses and strains are computed, and (3) then the topological sensitivity field is computed through Eq. (8); the resulting field is illustrated in Figure 9c.The interpretation is that regions of low sensitivity correspond to regions with relatively lower impact on performance (and can be removed). Similar topological sensitivity fields can be computed for various performance metrics, both in 2D and 3D [56].

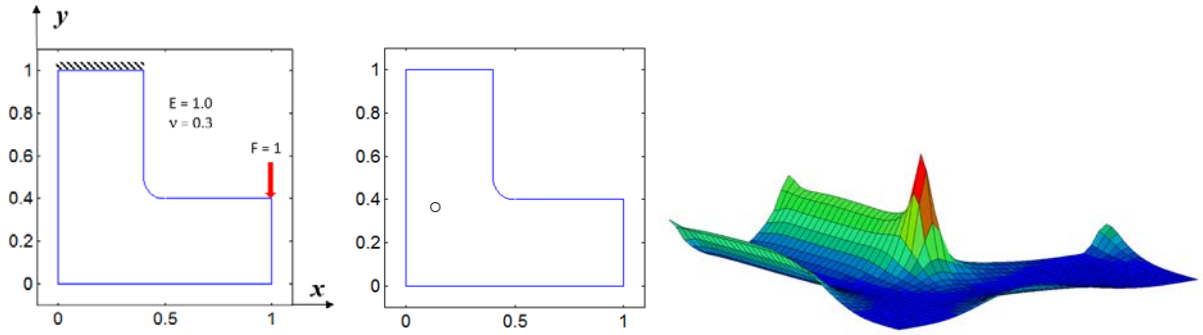
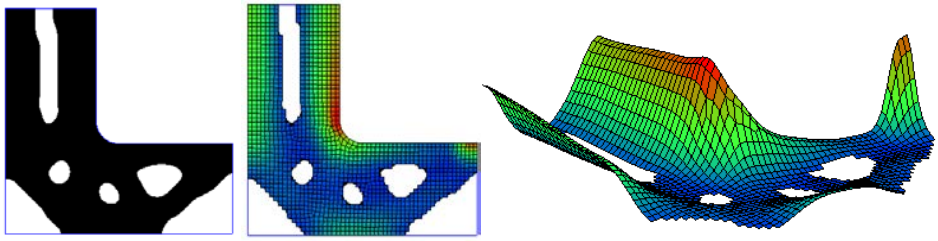


Figure 9: (a) A structural problem, (b) topological change, and (c) topological sensitivity field.

The PareTO method uses the topological sensitivity as a level-set to trace the Pareto curve for decreasing volume fraction. As the topology evolves, the topological sensitivity is recomputed at each iteration. For example, for an intermediate topology in Figure 10a, (1) FEA is carried over the new topology, (2) the stresses and strains are computed, and (3) the topological sensitivity field is computed through Eq. (8); the resulting topological sensitivity field is illustrated in Figure 10b and Figure 10c.


Figure 10: (a) Instance of topology, (b) compliance topological sensitivity (2D) (c) 3D view of (b).

3.5 Sensitivity of Support Volume based on Surface Angle

Analogous to the topological sensitivity for performance, we propose here topological sensitivity of support structure volume, i.e., "*the rate of change in support structure volume with respect to volumetric measure of the hole.*" Towards this end, consider the two scenarios illustrated in Figure 11, where the design is infinitesimally perturbed either in the interior, or on the boundary.

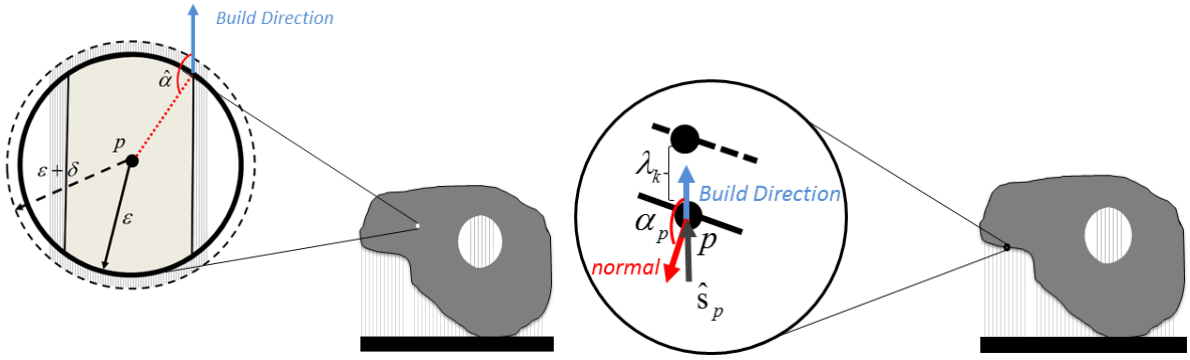


Figure 11: Sensitivity of support volume, (a) in the interior, (b) on boundary.

Interior Hole (Figure 11a): If a hole of radius ε is inserted in the interior of the domain (Ω_ε), one can compute the topological-shape sensitivity as follows. Employing the shape-sensitivity method proposed in [55], the topological derivative is computed via:

$$T_S(p \in \Omega) \equiv \lim_{\substack{\varepsilon \to 0 \\ \delta \to 0}} \frac{S(\Omega_{\varepsilon+\delta}) - S(\Omega_\varepsilon)}{V(B_{\varepsilon+\delta}) - V(B_\varepsilon)} \tag{9}$$

In Equation (9), $S(\Omega_\varepsilon)$ and $V(B_\varepsilon)$ are support volume and hole volume, for a hole of radius ε. Using the above definition, one can show that the support volume sensitivity is given by (see Figure 11a and Appendix):

$$\mathcal{T}_S(p \in \Omega) = \frac{3(\pi - \hat{\alpha} - \sin(\hat{\alpha})\cos(\hat{\alpha}))(\sin(\hat{\alpha}) - \frac{\sin^3(\hat{\alpha})}{3})}{\pi} \tag{10}$$

Where $\pi / 2 \leq \hat{\alpha} \leq \pi$ is the threshold angle. For example, if the threshold angle $\hat{\alpha} = \pi / 2$, then $\mathcal{T}_S(p) = 1$, i.e., the entire hole will need to be filled with support structures; a typical value is $\mathcal{T}_S(p \in \Omega) \approx 0.72$ when $\hat{\alpha} = 3\pi / 4$.

Boundary Hole (Figure 11b): Unlike the interior, the support volume on the boundary depends both on the local neighborhood (curvature) and the length and direction of support. In order to capture both, we define a scalar function $F^S(\mathrm{x}_p)$ at each boundary point as follows:

$$F^S(\mathrm{x}_p) = \frac{1}{2} l_p (1 - \cos(\alpha_p)) \tag{11}$$

In Equation (11), α_p is the angle between surface normal and build direction at boundary point p . We compute the sensitivity for the worst-case scenario, where boundary is perturbed along support at each point $\hat{\mathbf{s}}_p$. One can then show the sensitivity at the boundary is given by Equation (12):

$$\mathcal{T}_S(p \in \partial\Omega) = \frac{1}{2}(1 - \cos(\alpha_p)) \tag{12}$$

Further, for each overhang point, the same sensitivity value is assigned to its corresponding opposite point (see Figure 6).

Given the above definitions, one can compute the support volume sensitivity at all points; this is illustrated in Figure 12b and Figure 12c.

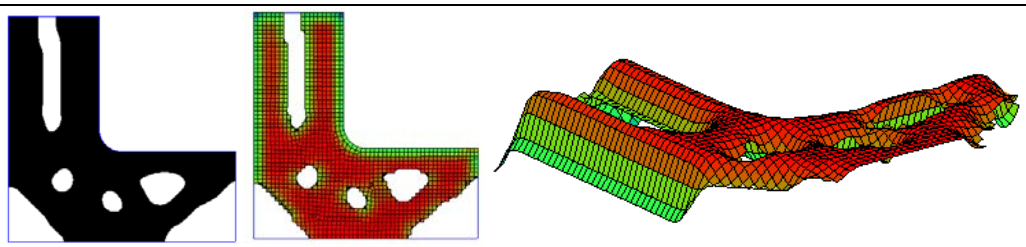


Figure 12: (a) Instance of topology. (b) Sensitivity of support volume (2D). (c) 3D view of (b).

3.6 Sensitivity Weighting

Once the performance and support volume sensitivities are computed and normalized, we exploit the well-established augmented Lagrangian method [57] to impose support structure constraint. Specifically, the support-constrained in Eq. (6) is first expressed in the standard form:

$$g = \frac{S(v)}{\eta S_{unc}(v)} - 1 \leq 0 \tag{13}$$

A popular method for imposing such constraints the augmented Lagrangian method [57], where the constraint and objective are combined to a single field:

$$\begin{aligned} \mathcal{L} &= J + \mathcal{L}_g \\ \mathcal{L}_g &= \begin{cases} \mu g + \frac{1}{2}\gamma(g)^2; & \mu + \gamma g > 0 \\ \frac{1}{2}\mu^2 \,/\, \gamma & \mu + \gamma g \leq 0 \end{cases} \end{aligned} \tag{14}$$

where μ is the Lagrangian multiplier and γ is the penalty parameter (that are updated during the optimization process [57]). By taking the topological derivative of Equation (14), we arrive at Equation (15) for the effective sensitivity [58], [59]:

$$\mathcal{T} = \mathcal{T}_J + w_S \mathcal{T}_S \tag{15}$$

where

$$w_S = \begin{cases} \mu + \gamma g & \mu + \gamma g > 0 \\ 0 & \mu + \gamma g \leq 0 \end{cases} \tag{16}$$

Observe that the weight on the support structure sensitivity is zero if $g < -\mu \,/\, \gamma$, else it takes a positive value. To illustrate Equation (15), suppose the two topological sensitivity fields are normalized to unity, and suppose $w_S = 1.0$, the resulting field is illustrated in Figure 13a and Figure 13b. Observe that the resulting field is a combination of the two fields in Figure 11 and

Figure 12. As the optimization progresses, the weight is determined dynamically from Equation (15), while the parameters μ and γ are updated during each iteration as described in [58], [59]. The algorithm is insensitive to the normalization/ scaling of the topological sensitivity fields, i.e., if the fields were not normalized, the computed parameters would be different, but the computed solutions would remain the same. Normalization, however, makes the implementation robust.

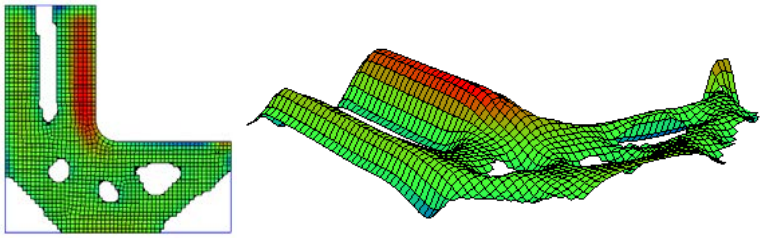


Figure 13: a) Equally weighted sum of the two sensitivity fields (2D) (b) 3D view of the sensitivity field

3.7 Topological Optimization Framework

Piecing these concepts together, the proposed algorithm proceeds as follows (see Figure 14):

1. It is assumed that the unconstrained optimization problem has been solved, and $S_{unc.}(v)$ has been computed.
2. Carry out FEA on Ω; compute the normalized sensitivity fields $\mathcal{T}_J$, $\mathcal{T}_S$, and the weighted field $\mathcal{T}$ as described above; smoothen the $\mathcal{T}$ field [60]. Observe that, every time the topology changes, FEA must be executed and the topological sensitivities recomputed.
3. Treating $\mathcal{T}$ as a level-set function, extract a new topology Ω using fixed-point iteration [60], and the iso-surface is extracted [61]. If the topology has not converged, repeat steps 2 and 3.
4. Decrement the volume fraction and return to step 2 until the desired volume is reached.

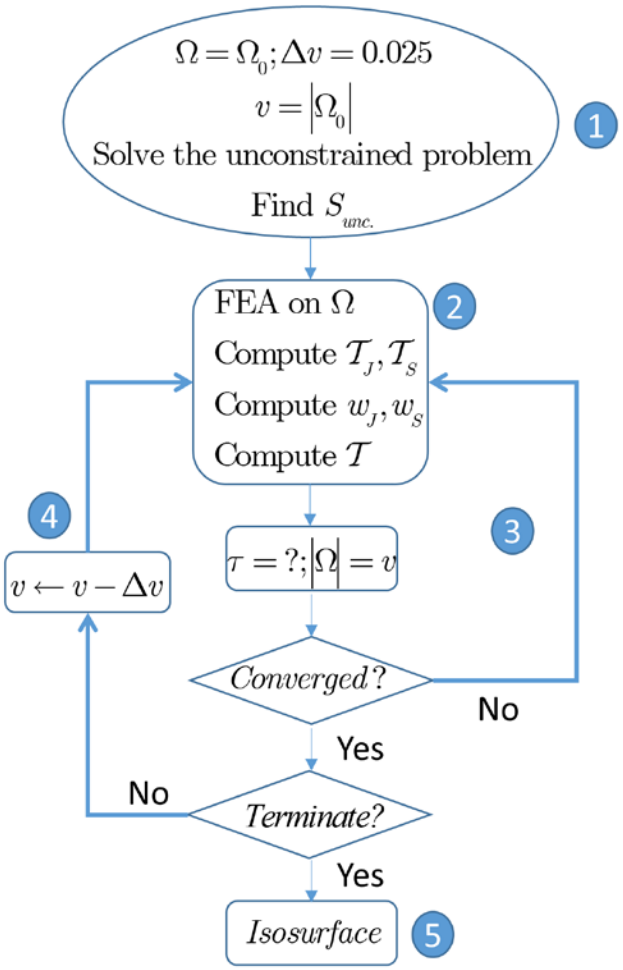


Figure 14: The proposed algorithm.

3.8 Limitations

The proposed sensitivity-based framework assumes a continuous dependence of support volume on boundary/topological perturbation. While this is generally true, the continuity is violated when the overhang angle approaches the critical limit at which the support volume abruptly drops to zero, making it non-differentiable. Due to this discontinuity, the proposed algorithm does not converge to solutions that may be obvious to a human designer. Instead, it converges to other solutions that can be reached in a smooth and continuous manner, as illustrated in the numerical experiments.

4. Numerical Experiments

In this section, we demonstrate the proposed method through several examples. In Section 4.1, we study the impact of the proposed method on the optimized design and support volume for a simple 2D example. In Section 4.2, the impact of user controlled parameter η is examined for the three-hole bracket. In Section 4.3, a more complex 3D design is optimized and the designs are printed to demonstrate the effectiveness of the proposed method. In section 4.4, the effect of build direction on support volume and performance are studied on a large-scale optimization problem. In all of the experiments, the material is assumed to be isotropic ABS plastic with Young's modulus of $E = 2\text{GPa}$ and Poisson ratio of $\nu = 0.39$. The threshold angle $\hat{\alpha}$ is assumed to be $3\pi/4$, unless otherwise noted.

4.1 2D MBB

Consider the 2D MBB design (implicit thickness of 1 cm) in Figure 15 whose support structure reduction was studied by Gaynor and Guest [16]. The initial design requires no support and the objective is to find stiffest design at 0.65 volume fraction.

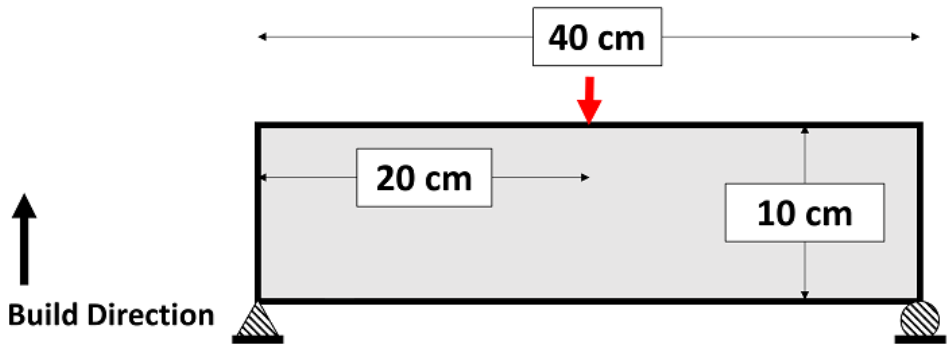


Figure 15: 2D MBB example with boundary conditions and build direction.

Recall that we first solve the unconstrained problem, and a series of topologies that lie on the Pareto curve are generated; see Figure 16.

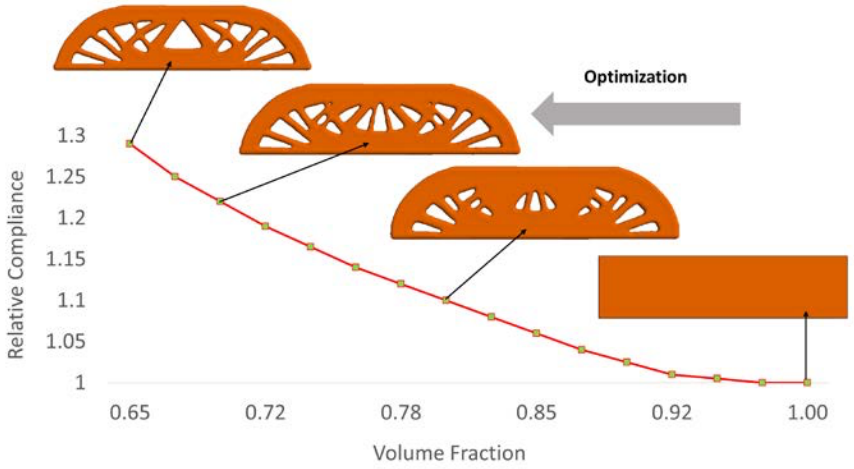


Figure 16: Compliance Pareto curve for the MBB beam.

Figure 17 illustrates the corresponding support volume in cm^3.

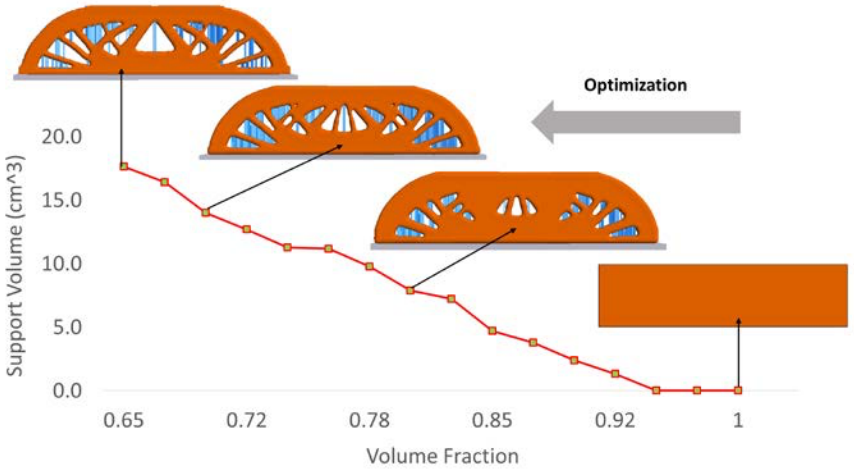
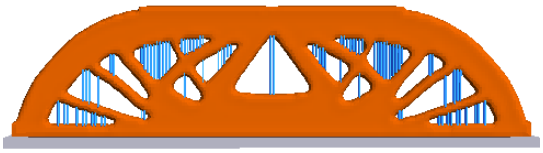
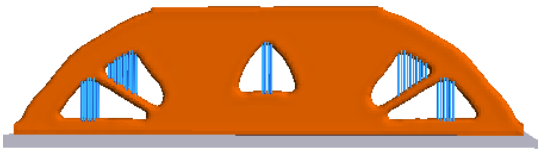


Figure 17: Support volume for the unconstrained MBB beam problem.

The unconstrained support volume from Figure 17 is then used as a reference to impose a support structure constraint. In particular, we study the impact of the relative constraint η (see Equation (6)) on the *final topology* at a volume fraction of 0.65. Table 1 summarizes the results; observe that with increased support structure constraint, the proposed method reduces the number of internal holes. This is, by no means, the unique solution to the problem; it happens to be a solution

that meets the desired constraints. It remains to be seen if one can generate topologies that meet the support structure constraint and exhibit a better performance.

Table 1: 2D MBB. Effect of support constraint on optimized design.

Final Topology	Support Volume Constraint	Support Volume Achieved	Relative Compliance
	–	–	1.29
	80%	62%	1.34
	60%	59%	1.42
	40%	42%	1.56
	0%	0%	1.75

4.2 Three-Hole Bracket

In this example, we study the impact of the support structure constraint over the entire Pareto curve. In particular, consider the three-hole bracket illustrated earlier in Figure 3. Recall the compliance Pareto curve for the unconstrained problem in Figure 4, and the corresponding support structure

curve in Figure 8. Figure 18 illustrates the Pareto curves for the unconstrained and the constrained case. As expected, imposing the support constraint increases compliance.

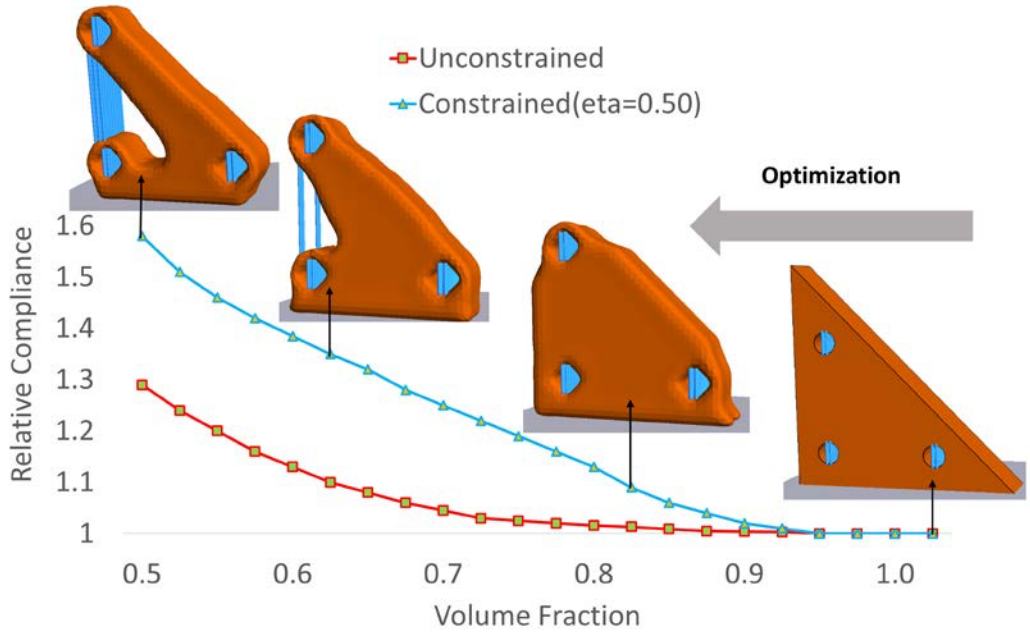


Figure 18: Unconstrained and constrained Pareto curves for three-hole bracket optimization.

Figure 19 illustrates the evolution of support structure volume for the two scenarios. Observe that as expected, removing more material can either increase or decrease the support volume due to its nonlinearity, nonetheless imposing a stringent constraint on support structure consistently reduces the support volume w.r.t the corresponding unconstrained design.

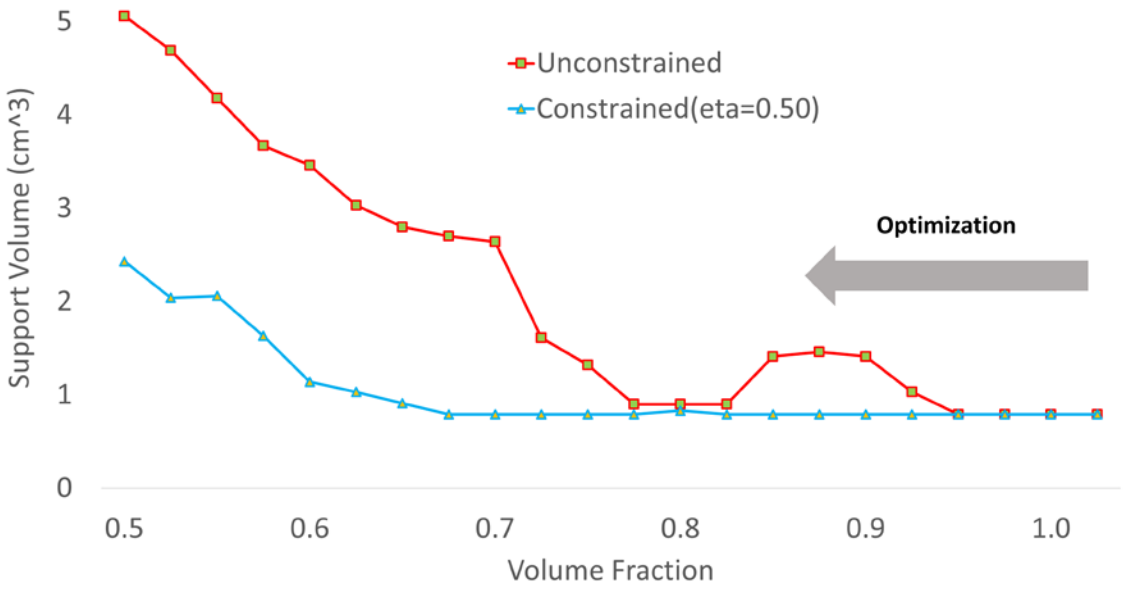


Figure 19: Evolution of support volume for three-hole bracket

The support volume prior to optimization is $S_0 = 0.79(cm^3)$. The objective is to find stiffest design at 0.5 volume fraction. Figure 20 illustrates the optimized design for (a) unconstrained, (b) constrained with $\eta = 0.50$. Relative compliance values for these cases are respectively 1.29 and 1.58.

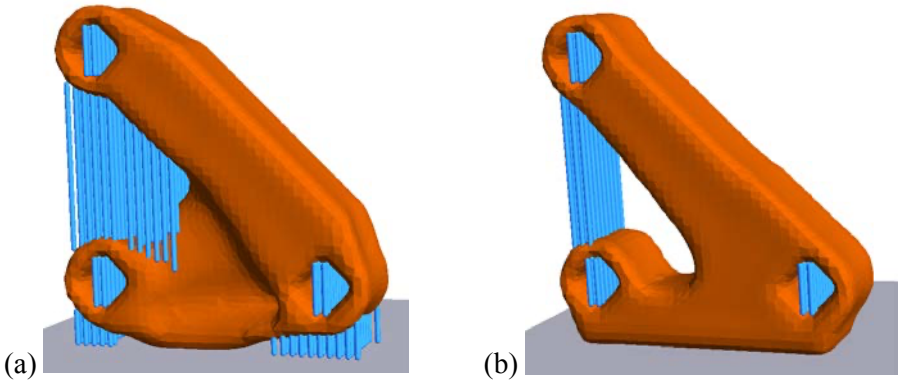


Figure 20: Optimized three-hole bracket. (a) Unconstrained (b) Constrained with $\eta = 0.50$.

4.3 Mount Bracket

Consider the mount bracket of Figure 21 subject to structural constraints and loading as illustrated. The threshold angle $\hat{\alpha}$ is assumed to be $3\pi / 4$. The build direction is illustrated in Figure 21 since it gives the best surface quality on the larger cylindrical face; for this design, prior to optimization the support volume is $S_0 = 1.12(cm^3)$. The objective is to find stiffest design at 0.7 volume fraction.

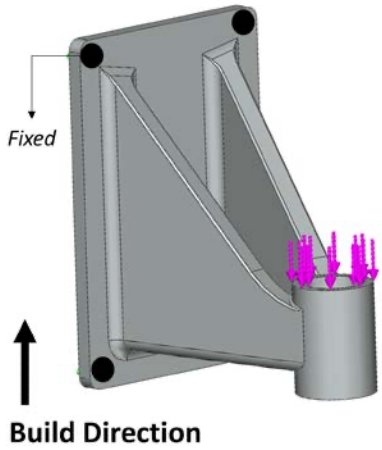


Figure 21: Mount bracket with boundary conditions and build direction

Figure 22 illustrates the optimized designs of (a) unconstrained and (b) constrained with $\eta = 0.80$. The final support structure volume for the unconstrained design is $9.24(cm^3)$ while for the constrained design it has reduced by about 17% to $7.70(cm^3)$.

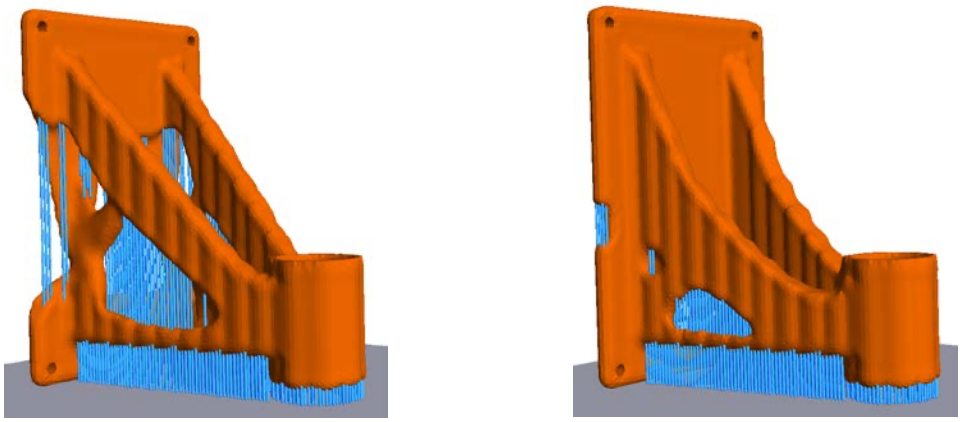


Figure 22: Optimized mount bracket at 0.7 volume fraction. (a) Unconstrained (b) $\eta = 0.80$.

Figure 23 illustrates the evolution of support volume throughout the optimization process. Observe that up to 0.9 volume fraction the unconstrained and constrained results are very similar. However for lower volume fractions the constrained support volume is consistently about 20% smaller than that of unconstrained design.

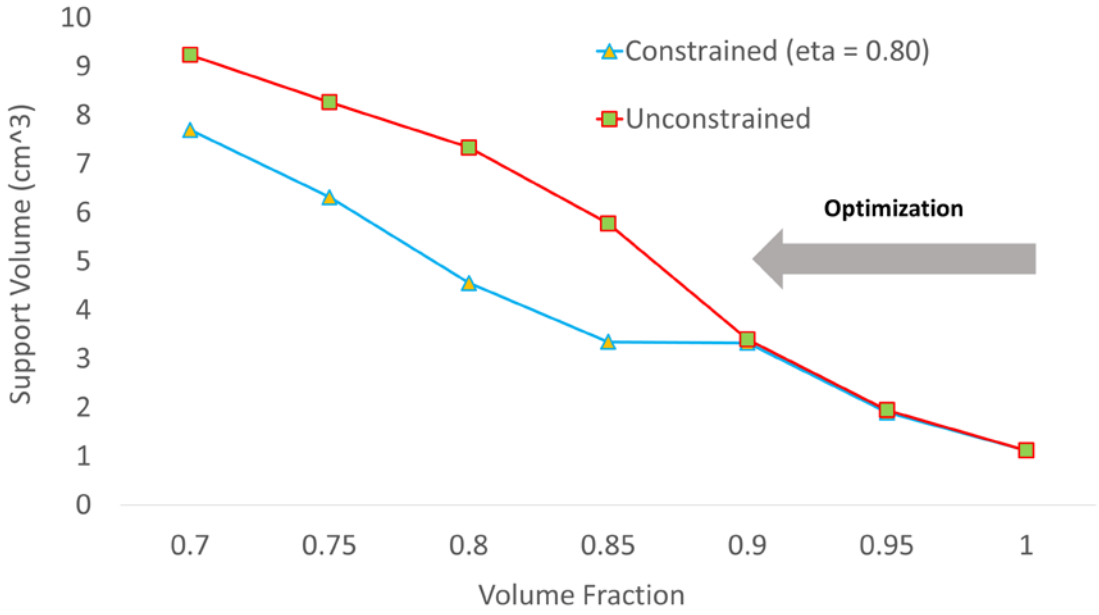


Figure 23: Evolution of support volume for the mount bracket.

Figure 24 illustrates the evolution of relative compliance values as more material is removed from the design. For the unconstrained design the final $(C \,/\, C_0)$ is about 1.05, while by imposing support constraint this value increases to about 2.52. Figure 24 highlights the trade-off between

support volume and compliance when the support constraint is imposed. It is essentially up to the designer to choose the intensity of support constraint.

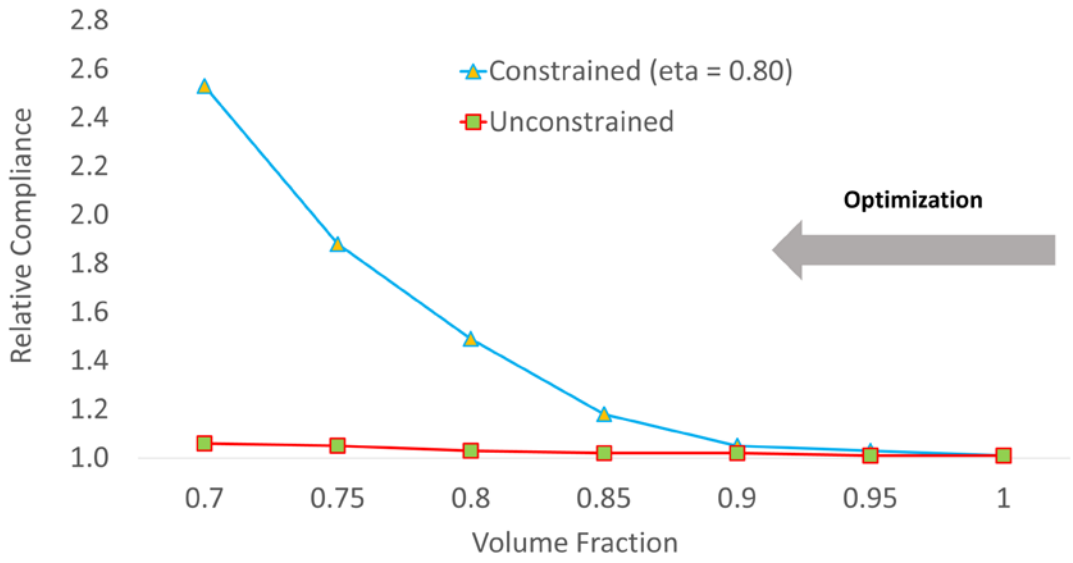


Figure 24: Evolution of compliance for the mount bracket.

To verify the validity of these simulated results, each of these topologies were 'printed' on an *XYZ Da Vinci 2.0* fused deposition printer. Note that the support structures were not generated by our algorithm, they were introduced by the XYZ software, based on default settings. Figure 25 illustrates the actual parts after clean-up. Observe that both of the optimized designs have the same weight (as prescribed by the optimization), while the amount of support structure is substantially reduced in the constrained design. This example illustrates the effectiveness of the proposed algorithm in handling support constraints.



Figure 25: Printed mount bracket and the required support structures at 0.7 volume fraction.

4.4 Different Build Directions

In this section, we demonstrate the robustness of the proposed method with respect to the build directions. Consider the problem posed in Figure 26 where the geometry is described via numerous curved surfaces and two cylindrical holes in two different directions; this makes picking the optimal build orientation challenging. Further to capture the complexity of the design, a hexahedral mesh with about 1.7 million degrees of freedom was used.

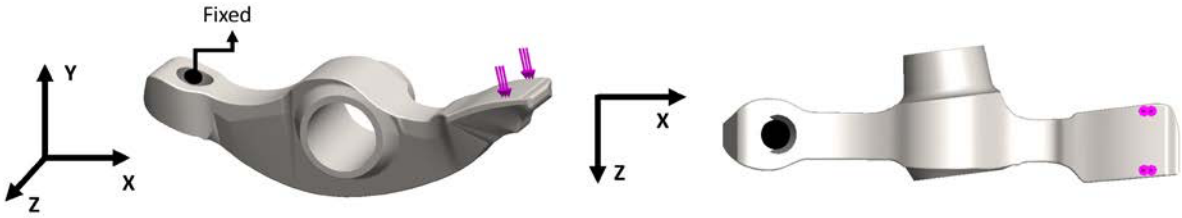


Figure 26: Rocker arm of Honda Supra-X 100 cc (grabcad.com): (a) Iso view, (b) Top view

A plausible choice for the build direction is –Z, as shown in Figure 27. In this direction, the larger cylinder has better surface quality and the initial support is minimal. First, we optimize the design for minimum compliance at 0.7 volume fraction without imposing any constraints on support structure.

In this particular orientation, $S_{unc.}(0.7)$ is smaller than S_0 , which means that during optimization, some of the overhanging surfaces are removed to reduce the overall support volume. Next, in order to further reduce support structure, we set $\eta = 0.90$ and solved the optimization problem of Eq. (6) to arrive at the design in Figure 27b. Observe that by imposing the support constraint, no additional overhangs are created, however since the initial design is dominant, support volume is reduced by only about 3%, while the compliance has increased by about 15%.

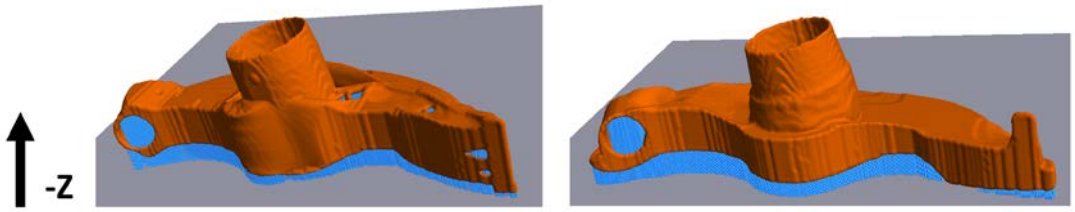


Figure 27: Rocker arm. Building in -Z direction a) unconstrained b) constrained

Next, the build direction was set to +Y since it gives better surface quality for the smaller cylindrical hole. Solving the same optimization problem as before results in the unconstrained design in Figure 28a and constrained design in Figure 28b with $\eta = 0.90$. The support volume was reduced by 20%, while the compliance increased by 32%.

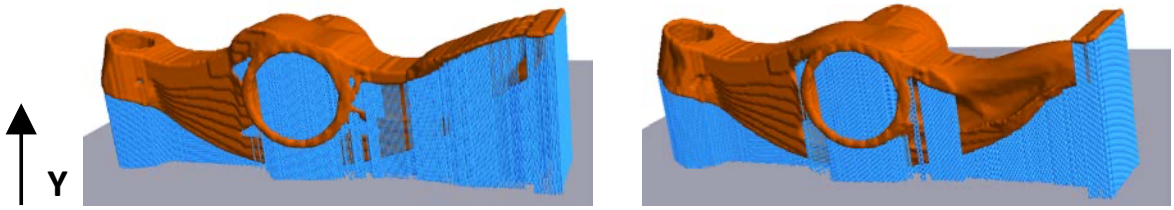


Figure 28: Build direction along +Y direction: (a) unconstrained, and (b) constrained.

Finally, the build direction was set to +X; a justification for this direction can be better fusion between layers, since the print area is smaller than previous directions. The results are summarized in Figure 29: the support volume was reduced by 4%, while the compliance increased by 10%.

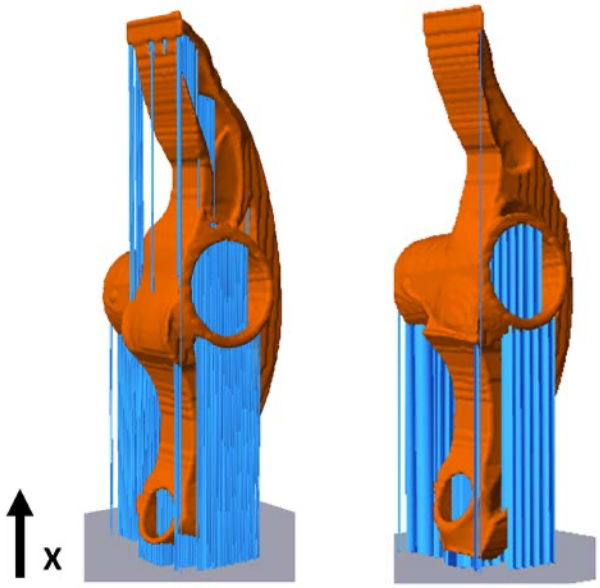


Figure 29: Rocker arm. Building in +X direction, unconstrained(left) and constrained (right)

4.5 Computational Cost

In this section, we study the convergence and performance of the proposed algorithm.

All experiments are conducted on a Windows 7 64 bit machine with an 8-core Intel Core i7 CPU running at 3.00 GHz, and 16 GB of memory.

Table 2 summarizes the CPU times of the unconstrained and constrained examples presented in sections 4.1 to 4.3. Observe that as the size of the problem and the support volume increases, the constrained problem requires more computational effort to compute support sensitivity field, yet for all of the presented experiments CPU time remains comparable.

Table 2: Computational cost, with and without support structure constraints.

Example	Finite element degrees of freedom	CPU time Unconstrained	CPU time Support Constrained
MBB	27,400	5.25 sec.	5.5 sec.
Three-hole bracket	45,012	10 sec.	$(\eta = 0.75)$ 11 sec. $(\eta = 0.50)$ 13.7 sec.
Mount bracket	196,965	1 min 18 sec.	1 min 29 sec.
Rocker Arm (-Z)	~1.7 million	28 min 30 sec.	30 min 59 sec.
Rocker Arm (+Y)	~1.7 million	28 min 30 sec.	32 min 6 sec.
Rocker Arm (+X)	~1.7 million	28 min 30 sec.	30 min 14 sec.

5. Summary and Future work

The main contribution of this paper is to propose a topology optimization framework that leads to designs with reduced support structures. Specifically, we introduced a novel topological sensitivity approach for constraining support structure volume during design optimization. The effectiveness of the proposed scheme was illustrated through several numerical examples, and demonstrated using FDM technology.

Support structures were assumed to be vertical for simplicity, but we believe that the methodology can be extended to handle non-vertical support structures. Additionally, the weighting proposed in this paper is simple and easy to implement. Since there are no benchmark examples in the literature for support volumes, it is difficult to evaluate efficacy of the proposed method.

Finally, the work presented is seen as a first step towards a more comprehensive framework for integrating topology optimization and additive manufacturing. Additional research is needed to include other AM-related constraints, such as surface roughness, volumetric error, inter-layer fusion, and so on. Finally, the proposed method must be coupled with methods for finding the optimum build direction to further reduce support volume.

Acknowledgements

The authors would like to thank the support of National Science Foundation through grants CMMI-1561899 and IIP-1500205.

Appendix

In this Appendix, we elaborate on the derivation of Eq. (10). Consider the hole inserted in the interior of the design, we need to find support volume $A = 4(A_1 + A_2)$.

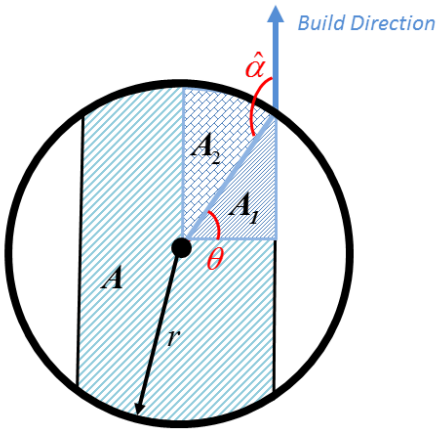


Figure 30: Support area in a 2D interior hole

Since $\theta = \hat{\alpha} - \pi / 2$ we have:

$$A_1 = \frac{1}{2}(r\cos(\theta))(r\sin(\theta)) = \frac{1}{2}r^2\sin(\theta)\cos(\theta) = \frac{-1}{2}r^2\sin(\hat{\alpha})\cos(\hat{\alpha}) \tag{17}$$

$$A_2 = \left(\frac{\pi/2 - \theta}{2\pi}\right)\pi r^2 = \frac{(\pi - \hat{\alpha})r^2}{2} \tag{18}$$

$$A = 2r^2(\pi - \hat{\alpha} - \sin(\hat{\alpha})\cos(\hat{\alpha})) \tag{19}$$

Next to find the support volume in a spherical ball with radius r we extend Eq. (19) as follows:

$$\begin{aligned} S &= \int_{-r\cos(\theta)}^{r\cos(\theta)} 2(r^2 - \mathrm{x}^2)(\pi - \hat{\alpha} - \sin(\hat{\alpha})\cos(\hat{\alpha}))dx \\ &= 4r^3(\pi - \hat{\alpha} - \sin(\hat{\alpha})\cos(\hat{\alpha}))(\sin(\hat{\alpha}) - \frac{\sin^3(\hat{\alpha})}{3}) \end{aligned} \tag{20}$$

Finally based on Eq. (9) the topological sensitivity is computed via Eq.(21):

$$\mathcal{T}_S(p \in \Omega) = \lim_{\substack{\varepsilon \to 0 \\ \delta \to 0}} \frac{4r^3(\pi - \hat{\alpha} - \sin(\hat{\alpha})\cos(\hat{\alpha}))(\sin(\hat{\alpha}) - \frac{\sin^3(\hat{\alpha})}{3})((\varepsilon + \delta)^3 - \varepsilon^3)}{\frac{4}{3}\pi((\varepsilon + \delta)^3 - \varepsilon^3)} \quad (21)$$

i.e.

$$\mathcal{T}_S(p \in \Omega) = \frac{3(\pi - \hat{\alpha} - \sin(\hat{\alpha})\cos(\hat{\alpha}))(\sin(\hat{\alpha}) - \frac{\sin^3(\hat{\alpha})}{3})}{\pi} \quad (22)$$

References

[1] H. A. Eschenauer and N. Olhoff, "Topology optimization of continuum structures: A review," *Applied Mechanics Review*, vol. 54, no. 4, pp. 331–389, 2001.

[2] G. I. N. Rozvany, "A critical review of established methods of structural topology optimization," *Structural and Multidisciplinary Optimization*, vol. 37, no. 3, pp. 217–237, 2009.

[3] M. Bendsøe and O. Sigmund, *Topology Optimization: Theory, Methods and Application*, 2nd ed. Springer, 2003.

[4] E. Kesseler, "Multidisciplinary design analysis and multi-objective optimisation applied to aircraft wing," *WSEAS transactions on systems and Control and Cybernetics*, vol. 1, no. 2, p. 221 227, 2006.

[5] J. J. Alonso, "Aircraft design optimization," *Mathematics and Computers in Simulation*, vol. 79, no. 6, pp. 1948–1958, 2009.

[6] V. H. Coverstone-Carroll, "Optimal multi-objective low-thrust spacecraft trajectories," *Comput. Methods Appl. Mech. Eng.*, vol. 186, pp. 387–402, 2000.

[7] L. Wang, "Automobile body reinforcement by finite element optimization," *Finite Elements in Analysis and Design*, vol. 40, no. 8, pp. 879–893, 2004.

[8] L. Harzheim, "A review of optimization of cast parts using topology optimization II-Topology optimization with manufacturing constraints," *Structural and Multidisciplinary Optimization*, vol. 31, no. 5, pp. 388–299, 2006.

[9] A. Krishnakumar and K. Suresh, "Hinge-Free compliant mechanism design via the Topological Level-Set," *Journal of Mechanical Design*, vol. 137, no. 3, 2015.

[10] I. Gibson, D. W. Rosen, and B. Stucker, *Additive Manufacturing Technologies*. Springer, 2010.

[11] H. Lipson and M. Kurman, *Fabricated: The New World of 3D Printing*. John Wiley, 2013.

[12] D. Brackett, I. Ashcroft, and R. Hague, "Topology optimization for additive manufacturing," in *22nd Annual international solid freeform fabrication symposium*, 2011, pp. 348–362.

[13] E. M. Dede, S. N. Joshi, and F. Zhou, "Topology Optimization, Additive Layer Manufacturing, and Experimental Testing of an Air-Cooled Heat Sink," *J. Mech. Des*, Jul. 2015.

[14] M. Leary, L. Merli, F. Torti, M. Mazur, and M. Brandt, "Optimal topology for additive manufacture: A method for enabling additive manufacture of support-free optimal structures," *Materials & Design*, vol. 63, pp. 678–690, Nov. 2014.
[15] K. Maute, A. Tkachuk, J. Wu, H. J. Qi, Z. Ding, and M. L. Dunn, "Level Set Topology Optimization of Printed Active Composites," *J. Mech. Des*, Jul. 2015.
[16] A. T. Gaynor and J. K. Guest, "Topology Optimization for Additive Manufacturing: Considering Maximum Overhang Constraint," presented at the 15th AIAA/ISSMO Multidisciplinary Analysis and Optimization Conference, Atlanta, GA, 2014, pp. 16–20.
[17] D. S. Thomas and S. W. Gilbert, "Costs and Cost Effectiveness of Additive Manufacturing: A Literature Review and Discussion." NIST, 2014.
[18] Z. Jibin, "Determination of optimal build orientation based on satisfactory degree theory for RPT," in *Ninth International Conference on Computer Aided Design and Computer Graphics, 2005*, 2005, p. 6 pp.-pp.
[19] P. M. Pandey, K. Thrimurthulu, and N. Venkata Reddy, "Optimal part deposition orientation in FDM by using a multicriteria genetic algorithm," *International Journal of Production Research*, vol. 42, no. 19, pp. 4069–4089, Oct. 2004.
[20] A. S. Nezhad, F. Barazandeh, A. R. Rahimi, and M. Vatani, "Pareto-Based Optimization of Part Orientation in Stereolithography," *Proceedings of the Institution of Mechanical Engineers, Part B: Journal of Engineering Manufacture*, vol. 224, no. 10, pp. 1591–1598, Oct. 2010.
[21] R. Paul and S. Anand, "Optimization of layered manufacturing process for reducing form errors with minimal support structures," *Journal of Manufacturing Systems*, 2014.
[22] P. Das, R. Chandran, R. Samant, and S. Anand, "Optimum Part Build Orientation in Additive Manufacturing for Minimizing Part Errors and Support Structures," 2015.
[23] X. Zhang, X. Le, A. Panotopoulou, E. Whiting, and C. C. L. Wang, "Perceptual Models of Preference in 3D Printing Direction," *ACM Trans. Graph.*, vol. 34, no. 6, p. 215:1–215:12, Oct. 2015.
[24]N. Umetani and R. Schmidt, "Cross-sectional structural analysis for 3d printing optimization," *SIGGRAPH Asia*, vol. 5, pp. 1–4, 2013.
[25] J. Vanek, J. A. G. Galicia, and B. Benes, "Clever Support: Efficient Support Structure Generation for Digital Fabrication," *Computer Graphics Forum*, vol. 33, no. 5, pp. 117–125, Aug. 2014.
[26] E. Barnett and C. Gosselin, "Weak Support Material Techniques For Alternative Additive Manufacturing Materials," *Additive Manufacturing*, 2015.
[27] J. Dumas, J. Hergel, and S. Lefebvre, "Bridging the Gap: Automated Steady Scaffoldings for 3D Printing," *ACM Trans. Graph.*, vol. 33, no. 4, p. 98:1–98:10, Jul. 2014.
[28] Y. Chen, K. Li, and X. Qian, "Direct Geometry Processing for Telefabrication Yong Chen, Kang Li and Xiaoping Qian," *J. Comput. Inf. Sci. Eng*, vol. 13, no. 4, 2013.
[29] A. Gebhardt, "Additive Manufacturing Design and Strategies," in *Understanding Additive Manufacturing*, A. Gebhardt, Ed. Hanser, 2011, pp. 103–128.
[30] I. Gibson, G. Goenka, R. Narasimhan, and N. Bhat, "Design rules for additive manufacture," in *International Solid Free Form Fabrication Symposium*, 2010.
[31] L. Liu, C. Wang, A. Shamir, and E. Whiting, "3D printing oriented design: geometry and optimization," in *SIGGRAPH Asia 2014 Courses*, 2014, p. (Presentation).

[32] C. C. Seepersad, T. Govett, K. Kim, M. Lundin, and D. Pinero, "A designer's guide for dimensioning and tolerancing SLS parts," in *Solid Freeform Fabrication Symposium, Austin, TX*, 2012, pp. 921–931.
[33] C. B. Williams and C. C. Seepersad, "Design for additive manufacturing curriculum: A problem-and project-based approach," in *International solid freeform fabrication symposium*, 2012, pp. 81–92.
[34] M. Zhou, R. Fleury, Y.-K. Shyy, H. Thomas, and J. Brennan, "Progress in Topology Optimization with Manufacturing Constraints," 2002.
[35] Q. Xia, T. Shi, M. Y. Wang, and S. Liu, "Simultaneous optimization of cast part and parting direction using level set method," *Struct Multidisc Optim*, vol. 44, no. 6, pp. 751–759, Aug. 2011.
[36] W. Wang, T. Y. Wang, Z. Yang, L. Liu, X. Tong, W. Tong, J. Deng, F. Chen, and X. Liu, "Cost-effective printing of 3D objects with skin-frame structures," *ACM Transactions on Graphics*, vol. 32, no. 6, pp. 1–10, Nov. 2013.
[37] K. Hu, S. Jin, and C. C. L. Wang, "Support slimming for single material based additive manufacturing," *Computer-Aided Design*, vol. 65, pp. 1–10, Aug. 2015.
[38] O. Sigmund, "A 99 line topology optimization code written in Matlab," *Structural and Multidisciplinary Optimization*, vol. 21, no. 2, pp. 120–127, 2001.
[39] A. Rietz, "Sufficiency of a finite exponent in SIMP (power law) methods," *Structural and Multidisciplinary Optimization*, vol. 21, no. 2, pp. 159–163, 2001.
[40] J. Du, "Topology Optimization of Continuum Structures with Respect to Simple and Multiple Eigenfrequencies," in *6th World Congresses of Structural and Multidisciplinary Optimization*, Rio de Janeiro, 2005.
[41] M. Zhou and G. I. N. Rozvany, "The COC algorithm, part II: Topological, geometry and generalized shape optimization.," *Computer Methods in Applied Mechanics and Engineering*, vol. 89, no. 1–3, pp. 309–336, 1991.
[42] G. Allaire and F. Jouve, "A level-set method for vibration and multiple loads structural optimization," *Structural and Design Optimization*, vol. 194, no. 30–33, pp. 3269–3290, 2005.
[43]M. Y. Wang, X. Wang, and D. Guo, "A level set method for structural topology optimization," *Computer Methods in Applied Mechanics and Engineering*, vol. 192, pp. 227–246, 2003.
[44] X. Wang, "Structural shape and topology optimization in a level-set-based framework of region representation," *Structural and Multidisciplinary Optimization*, vol. 27, no. 1–2, pp. 1–19, 2004.
[45] X. Huang and Y. M. Xie, "A new look at ESO and BESO optimization methods," *Structural and Multidisciplinary Optimization*, vol. 35, no. 1, pp. 89–92, 2008.
[46] K. Suresh, "A 199-line Matlab code for Pareto-optimal tracing in topology optimization," *Structural and Multidisciplinary Optimization*, vol. 42, no. 5, pp. 665–679, 2010.
[47] K. Suresh, "Efficient Generation of Large-Scale Pareto-Optimal Topologies," *Structural and Multidisciplinary Optimization*, vol. 47, no. 1, pp. 49–61, 2013.
[48] A. M. Mirzendehdel and K. Suresh, "A Pareto-Optimal Approach to Multimaterial Topology Optimization," *Journal of Mechanical Design*, vol. 137, no. 10, 2015.
[49] J. Céa, S. Garreau, P. Guillaume, and M. Masmoudi, "The shape and topological optimization connection," *Computer Methods in Applied Mechanics and Engineering*, vol. 188, no. 4, pp. 713–726, 2000.

[50] Y. Jiang, H. Kautz, and B. Selman, "Solving problems with hard and soft constraints using a stochastic algorithm for MAX-SAT," in *Proceedings of the 1st International Workshop on Artificial Intelligence and Operations Research*, Timberline, Oregon, 1995.
[51] A. A. Novotny, "Topological-Shape Sensitivity Method: Theory and Applications," *Solid Mechanics and its Applications*, vol. 137, pp. 469–478, 2006.
[52] J. Sokolowski and A. Zochowski, "On Topological Derivative in Shape Optimization," *SIAM journal on control and optimization*, vol. 37, no. 4, pp. 1251–1272, 1999.
[53] A. A. Novotny, R. A. Feijoo, and E. Taroco, "Topological Sensitivity Analysis for Three-dimensional Linear Elasticity Problem," *Computer Methods in Applied Mechanics and Engineering*, vol. 196, no. 41–44, pp. 4354–4364, 2007.
[54] I. Turevsky and K. Suresh, "Generalization of Topological Sensitivity and its Application to Defeaturing," in *ASME IDETC Conference*, Las Vegas, 2007.
[55] R. A. Feijoo, A. A. Novotny, E. Taroco, and C. Padra, "The topological-shape sensitivity method in two-dimensional linear elasticity topology design," in *Applications of Computational Mechanics in Structures and Fluids*, CIMNE, 2005.
[56] K. Suresh and M. Takalloozadeh, "Stress-Constrained Topology Optimization: A Topological Level-Set Approach," *Structural and Multidisciplinary Optimization*, vol. 48, no. 2, pp. 295–309, 2013.
[57] J. Nocedal and S. Wright, *Numerical Optimization*. Springer, 1999.
[58] S. Deng and K. Suresh, "Multi-constrained 3D topology optimization via augmented topological level-set," *Computers and Structures*, vol. 170, no. 1, pp. 1–12, 2016.
[59] S. Deng and K. Suresh, "Multi-constrained topology optimization via the topological sensitivity," *Structural and Multidisciplinary Optimization*, vol. 51, no. 5, pp. 987–1001, 2015.
[60] K. Suresh, "Efficient Generation of Large-Scale Pareto-Optimal Topologies," *Structural and Multidisciplinary Optimization*, vol. 47, no. 1, pp. 49–61, 2013.
[61] W. E. Lorensen and H. E. Cline, "Marching Cubes: a high resolution 3D surface reconstruction algorithm.," *Computer Graphics (Proc. of SIGGRAPH)*, vol. 21, no. 4, pp. 163–169, 1987.

View publication stats